Original Article

Radiomics with structural magnetic resonance imaging, surface morphometry features, neurology scales, and clinical metrics to evaluate the neurodevelopment of preschool children with corrected tetralogy of Fallot

Feng Yang[1#], Jingjing Zhong[1#], Peng Liu[1], Wei Yu[1], Yuting Liu[2], Meijiao Zhu[1], Ming Yang[1], Xuming Mo[3]

[1]Department of Radiology, Children's Hospital of Nanjing Medical University, Nanjing, China; [2]Nanjing University, Nanjing, China; [3]Department of Cardiothoracic Surgery, Children's Hospital of Nanjing Medical University, Nanjing, China

Contributions: (I) Conception and design: F Yang, M Yang, X Mo; (II) Administrative support: W Yu, J Zhong; (III) Provision of study materials or patients: P Liu, Y Liu, M Zhu; (IV) Collection and assembly of data: All authors; (V) Data analysis and interpretation: F Yang; (VI) Manuscript writing: All authors; (VII) Final approval of manuscript: All authors.

[#]These authors contributed equally to this work as co-first authors.

Correspondence to: Ming Yang, MD, PhD. Department of Radiology, Children's Hospital of Nanjing Medical University, 72 Guangzhou Road, Nanjing 210008, China. Email: yangming19710217@163.com.

Background: Despite the improved survival rates of children with tetralogy of Fallot (TOF), various degrees of neurodevelopmental disorders persist. Currently, there is a lack of quantitative and objective imaging markers to assess the neurodevelopment of individuals with TOF. This study aimed to noninvasively examine potential quantitative imaging markers of TOF neurodevelopment by combining radiomics signatures and morphological features and to further clarify the relationship between imaging markers and clinical neurodevelopment metrics.

Methods: This study included 33 preschool children who had undergone surgical correction for TOF and 29 healthy controls (36 in the training cohort and 26 in the testing cohort), all of whom underwent three-dimensional T1-weighted high-resolution (T1-3D) head magnetic resonance imaging (MRI). Radiomics features were extracted by Pyradiomics to construct radiomics models, while surface morphometry (surface and volumetric) features were analyzed to build morphometry models. Merged models integrating radiomics and morphometry features were subsequently developed. The optimal discriminative radiomics signatures were identified via least absolute shrinkage and selection operator (LASSO). Machine learning classification models include support vector machine (SVM) with radial basis function (RBF) and multivariable logistic regression (MLR) models, both of which were used to evaluate the potential imaging biomarkers. Performances of models were evaluated based on their calibration and classification metrics. The area under the receiver operating characteristic curves (AUCs) of the models were evaluated using the Delong test. Neurodevelopmental assessments for children with corrected TOF were conducted with the Wechsler Preschool and Primary Scale of Intelligence-Fourth Edition (WPPSI-IV). Furthermore, the correlation of the significant discriminative indicators with clinical metrics and neurodevelopmental scales was evaluated.

Results: Twelve discriminative radiomics signatures, optimized for classification, were identified. The performance of the merged model (AUCs of 0.922 and 0.917 for the training set and test set with SVM, respectively) was superior to that of the single radiomics model (AUCs of 0.915 and 0.917 for the training set and test set with SVM, respectively) and that of the single morphometric models (AUCs of 0.803 and 0.756 for the training set and test set with SVM, respectively). The radiomics model demonstrated higher significance than did the morphometric models in training set with SVM (AUC: 0.915 *vs.* 0.803; P<0.001). Additionally, the significant indicators showed a correlation with clinical indicators and neurodevelopmental scales.

Conclusions: MRI-based radiomics features combined with morphometry features can provide

complementary information to identify neurodevelopmental abnormalities in children with corrected TOF, which will provide potential evidence for clinical diagnosis and treatment.

Keywords: Radiomics; magnetic resonance imaging (MRI); machine learning; tetralogy of Fallot (TOF); neurodevelopment

Submitted Jun 05, 2024. Accepted for publication Sep 03, 2024. Published online Sep 26, 2024.
doi: 10.21037/tp-24-219
View this article at: https://dx.doi.org/10.21037/tp-24-219

Introduction

Tetralogy of Fallot (TOF), the most prevalent form of cyanotic congenital heart disease (CHD), comprises four anatomical abnormalities: ventricular septal defect (VSD), pulmonary stenosis, right ventricular hypertrophy, and an overriding aorta (ORA). TOF is one of the most common cyanotic heart defects, accounting for approximately 7–10% of all CHD cases. The incidence of TOF is estimated to be about 1 in 3,000 live births (1). Despite significant improvements in the long-term survival rate of children with CHD due to advancements in medical care (2-7), Children with TOF still experience neurodevelopmental disorders (NDDs), including impairments in language, memory, attention, and executive function, which can potentially impact the long-term growth and development. These disorders are thought to be associated with several factors, including chronic hypoxemia due to reduced oxygenated blood flow, surgical interventions, and genetic abnormalities. The precise mechanism underlying neurodevelopmental impairments in children with CHD remains unclear (8-10) and may involve impaired cerebral oxygen delivery, altered brain maturation, and potential neuroinflammatory responses. Currently, the clinical assessment of neurodevelopment in children with CHD is relatively subjective and lacks objective quantitative diagnostic markers. Understanding these mechanisms is crucial for improving the long-term neurodevelopmental outcomes of children with TOF. Therefore, studying the brain development of children with TOF and identifying influential markers can enhance the monitoring of neurodevelopment. This can facilitate the implementation of appropriate and timely intervention measures to improve their quality of life (5).

Radiomics can be used to extract valuable quantitative information from medical images (11,12), and then learning or deep learning models can be employed for prediction and analysis. The potential means of discrimination can be discovered and clinical mechanisms can be revealed (13-16). Moreover, the in-depth information will provide more accurate evidence for clinical decision-making. Radiomics has been applied to various clinical decisions, diagnostic, and prognostic assessments (17-23). In recent years, there has been a growing utilization of radiomics in neurodevelopment. Several studies have demonstrated that radiomics information can provide valuable insights into NDDs and aid in the diagnosis and treatment within

Highlight box

Key findings

- This study identified 12 significant discriminative radiomics signatures optimized for the evaluation of neurodevelopmental abnormalities in preschool children with corrected tetralogy of Fallot (TOF).
- A combined model incorporating radiomics and surface morphometry features showed superior performance (area under the receiver operating characteristic curve: 0.922 in the training set and 0.917 in the testing set) compared to individual radiomics or morphometric models.

What is known and what is new?

- It is known that children with corrected TOF face persistent neurodevelopmental challenges despite improved survival rates.
- This study developed a novel combination of radiomics and surface morphometry models from structural magnetic resonance imaging (MRI) to quantitatively assess neurodevelopment in TOF children, which demonstrated potential for noninvasive neurodevelopmental assessment.

What is the implication, and what should change now?

- The combined radiomics and morphometry imaging approach offers a promising new method for identifying neurodevelopmental abnormalities in children with corrected TOF. This could lead to more targeted clinical interventions and improved follow-up care.
- Future clinical protocols should consider integrating quantitative imaging biomarkers derived from radiomics and morphometry analysis in MRI assessments for the development of children with congenital heart diseases such as TOF.

clinical settings. Shin *et al.* applied a radiomics approach to predict adverse psychomotor development in preterm infants based on brain magnetic resonance imaging (MRI), showing that MRI-based radiomics analysis can predict adverse psychomotor outcomes in preterm infants (24). Another study conducted by Wagner *et al.* combined clinical parameters and radiomics features to predict adverse neurodevelopmental outcomes of extremely preterm neonates (25). Research on the diagnosis of attention-deficit/hyperactivity disorder (ADHD) demonstrated that MRI radiomic features are potential diagnostic biomarkers of ADHD (26). Additionally, a study by Wang *et al.* predicted adverse motor outcomes for neonates with punctate white-matter lesions using MRI radiomics (27). These examples highlight the effective applications of radiomics in exploring neurodevelopmental conditions in children.

Structural MRI (sMRI) has become a crucial tool in medical imaging due to its ability to provide high-resolution images of soft tissues without radiation, making the noninvasive observation of brain structures possible. Its short scan time, high patient compliance, and accessibility have led to its widespread use in studies of brain development. Previous research has demonstrated the value of sMRI in various neurological conditions (28). For example, Shin *et al.* (29) used cortical thickness measurements from sMRI combined with machine learning to predict the conversion from mild cognitive impairment in Parkinson disease, illustrating the predictive power of sMRI in neurodegenerative conditions. sMRI can also reveal brain structure alteration in children with CHD. Morton *et al.* (30) identified that brain sulcus characteristics in children with TOF could serve as markers for neurodevelopmental risk. Meanwhile, Aleksonis *et al.* (31) reviewed relationships between structural neuroimaging and neurocognitive outcomes in adolescents and young adults with CHD, finding a correlation between worse brain structure and poorer cognitive performance. Dhari *et al.* (32) examined the impact of cardiopulmonary bypass (CPB) on neurogenesis and cortical maturation, while Claessens *et al.* (33) reported brain microstructural development with critical CHD based on sMRI. Additionally, a previous study using fetal brain volume predicted subsequent neurodevelopmental outcomes in children with CHD (34). These findings highlight the importance of sMRI in understanding and predicting neurodevelopmental outcomes in children with CHD and suggest its potential as a valuable tool in clinical research.

Therefore, various studies have been conducted based on sMRI to measure brain volume, cortical thickness, and other structural characteristics that indicate a developmental delay in children with CHD. However, most of this research has focused on superficial qualitative morphometric features of images, such as volume, surface area, and thickness, while often neglecting the more nuanced quantitative features that radiomics can provide. Radiomics can extract a large number of quantitative features from medical images, capturing subtle patterns and details not visible to the naked eye, including first-order statistics (e.g., histogram-based features such as mean intensity and variance), shape-based features (e.g., sphericity and surface area), and texture features [e.g., gray-level co-occurrence matrix (GLCM), which describes the spatial relationship between pixels]. Additionally, higher-order features derived from transformations such as wavelets can capture more complex patterns. These in-depth quantitative radiomic features are obtained through advanced image-processing techniques and can provide a more comprehensive assessment of brain structure. Therefore, in our study, we combined potential quantitative radiomics features with morphometry features to examine the neurodevelopment of children with TOF.

We identified potential imaging markers of TOF in preschool children based on radiomics combined with sMRI surface morphometric features, integrating machine learning models to examine the neurodevelopment of TOF. We then determined the correlation between imaging markers and clinical neurodevelopment metrics to advance intervention in the neurodevelopment of children with CHD and to improve the quality of life of children with TOF. We present this article in accordance with the TRIPOD reporting checklist (available at https://tp.amegroups.com/article/view/10.21037/tp-24-219/rc).

Methods

Participants

In this study, 36 children with TOF who underwent CPB thoracotomy and 29 normal controls with an equal sex ratio, education level, and age were retrospectively recruited from June 2019 to October 2023. The inclusion criteria for children with TOF were as follows: (I) aged between 3 and 6 years (preschool age, nonpreterm); (II) without congenital or metabolic diseases except TOF with pulmonary stenosis; (III) without central nervous system diseases, such as tumor or trauma; (IV) no history of psychiatric disease or psychotropic drug treatment; and (V) right-handedness.

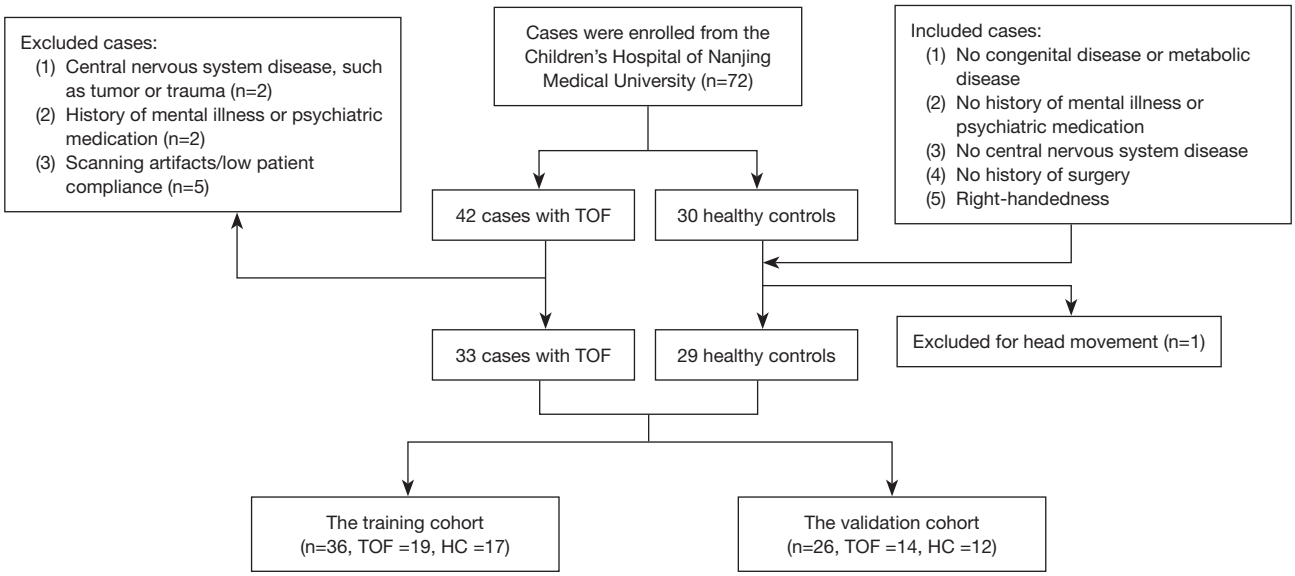

Figure 1 The flowchart of participant recruitment in this study. TOF, tetralogy of Fallot; HC, healthy control.

Normal controls included (I) transient fever outpatients (healthy after follow-up) (II) children receiving regular physical examinations at children's health clinics, and (III) volunteers from society. The inclusion criteria of normal controls were as follows: (I) no congenital or metabolic disease, (II) no history of psychiatric disease or psychotropic medication, (III) no central nervous system disease, (IV) no history of surgery, and (V) right-handedness; meanwhile, the exclusion criterion was contraindications to MRI examination. Three children with TOF were excluded due to low MRI quality. The images were then reviewed by two experienced pediatric neuroradiologists, blinded to the details of each participant's medical history. If there was a difference in opinion, consensus was reached through discussion. The cases were randomly divided into a training set and a validation set at a 6:4 ratio (36 in the training cohort and 26 in the testing cohort). *Figure 1* is the flowchart of participant recruitment in this study.

The study was conducted in accordance with the Declaration of Helsinki (as revised in 2013). The study was approved by the Ethics Committee of the Children's Hospital of Nanjing Medical University (No. 201907212-1), and informed consent was obtained from all the patients' parents or legal guardians.

Clinical metrics and neurodevelopmental assessment

The Chinese version of the Wechsler Preschool and Primary Intelligence Scale Fourth Edition (WPPSI-IV) was used to evaluate the neurodevelopmental outcomes of children in the TOF group (preschool, aged between 3 and 6 years) (35). The scale can test the verbal comprehension index (VCI), the visual-spatial index (VSI), the working memory index (WMI), and the full-scale intelligence quotient (FSIQ; scores with an expected average of 100). The VCI represents the capacity for language processing, such as understanding, reasoning, and communication. The VSI evaluates nonverbal abilities related to the analysis and organization of visual patterns. The WMI indicates the ability to temporarily hold and manipulate information.

In addition, several crucial clinical metrics including body mass index (BMI), McGoon index (a clinical measurement used to assess the adequacy of the pulmonary arteries in patients with congenital heart defects), ORA, pulse oxygen saturation (SpO_2), VSD, CPB time, and aortic cross-clamp (ACC) time were collected from the electronic medical records. Questionnaires were completed for the assessment of maternal education (ME), socioeconomic level (SEL), and maternal age at pregnancy (MAP), as these are typically associated with neurodevelopmental outcomes. The demographic indicators, age, and gender of the children were also recorded.

MRI parameters

All participants underwent a head 3-T MRI (Ingenia 3.0,

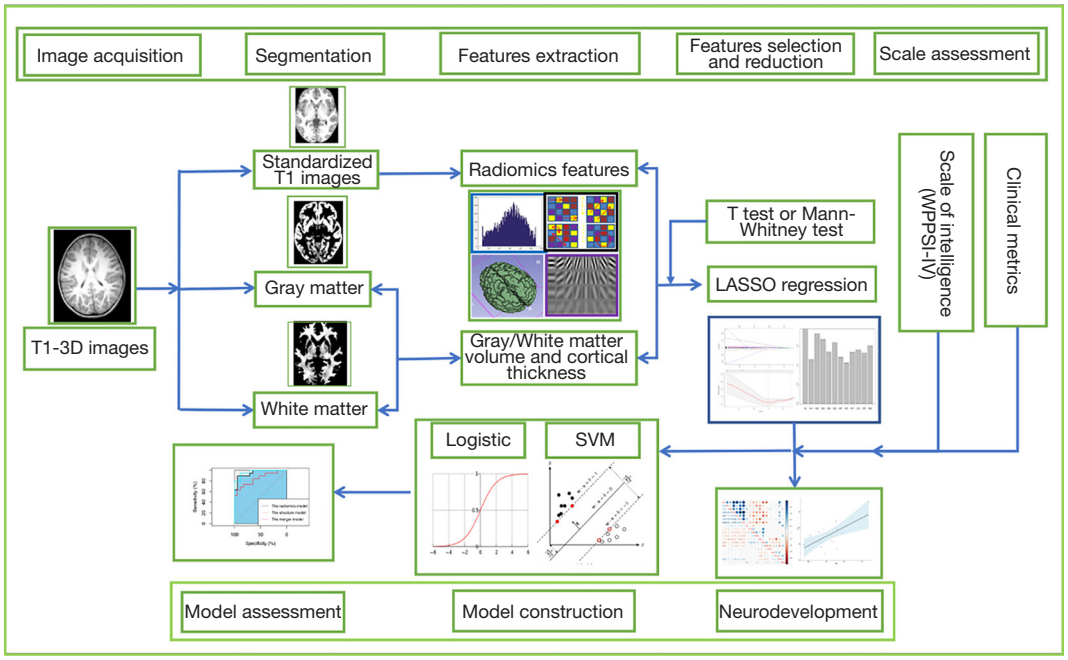

Figure 2 The radiomics workflow for integrative analysis of TOF neurodevelopment. TOF, tetralogy of Fallot; SVM, support vector machine; LASSO, least absolute shrinkage and selection operator; WPPSI-IV, Wechsler Preschool and Primary Intelligence Scale Fourth Edition.

Philips, Amsterdam, the Netherlands) scans with 32-channel head coils in the Radiology Department of the Children's Hospital of Nanjing Medical University. All participants were required to stay awake for 8 hours before the MRI. Scans were conducted at night, either during natural sleep or under chloral hydrate sedation (1 mL/kg) with parental consent. Earplugs were used to mitigate scanning noise, and head restraints were applied to limit head motion. The specific parameters of high-resolution T1-weighted three-dimensional (3D) imaging were as follows: time to echo (TE) =3.5 ms, time to repetition (TR) =7.9 ms, a field of view (FOV) =200 mm × 200 mm × 200 mm, slice thickness =1 mm, and acquisition time =4 min and 24 s. Conventional axial T2-weighted images were acquired to exclude brain injury under the following parameters: TE =110 ms, TR=4,000 ms, FOV =200 mm × 200 mm × 119 mm, slice thickness =5 mm, and acquisition time =1 min and 28 s.

Image preprocessing

For the morphometry features, the raw Digital Imaging and Communications in Medicine (DICOM) images are first converted to Neuroimaging Informatics Technology Initiative (NIfTI) format using DCM2NII (https://people.cas.sc.edu/rorden/mricron/dcm2nii.html/). Preprocessing was then performed to obtain standardized gray-matter volume (GMV) images, standardized white-matter volume (WMV) images, and standardized T1 images based on MATLAB (R2013b) toolbox Computational Anatomy Toolbox 12 (36) (CAT12) version 12.1 (http://www.neuro.uni-jena.de/cat/) and Statistical Parameter Mapping 12 (SPM12; https://www.fil.ion.ucl.ac.uk/spm/software/spm12/). After the preprocessed images were aligned to the Montreal Neurological Institute 152 (MNI152) template space, the cortical thickness was calculated from the normalized images, with a 20.0-mm full-width-at-half-maximum (FWHM) Gaussian kernel.

For the radiomics features, first, N4 bias-field correction was carried out in SimpleITK version 2.0.2 (http://simpleitk.org/) a package from Python version 3.7.6 to normalize the gray level of all MRIs. The voxel size was resampled to 1 mm × 1 mm × 1 mm. Gaussian filtering was applied with the sigma set at values of 0.5, 1.0, and 1.5. z-score normalization was performed on data after feature extraction. An overview of our workflow is illustrated in *Figure 2*.

Segmentation and feature extraction

Morphological features (surface and volumetric metrics) and radiomic features were extracted from the preprocessed images.

Each structural image underwent segmentation into gray matter, white matter (WM), and cerebrospinal fluid (CSF), followed by normalization to the MNI template space. Following this, volumetric metrics, including mean WMV, mean GMV, CSF, and total intracranial volume (TIV), surface features, and cortical thickness, were extracted based on SPM and CAT12.

Two experienced physicians delineated the 3D brain T1-weighted MRI images layer by layer (CSF removed) as regions of interest (ROIs) using an open-source software package (3D-Slicer version 5.0.2; https://www.slice r.org). Furthermore, radiomics features of ROI were obtained with Pyradiomics (https://pyradiomics.readthedocs.io/en/latest/features.html). All features were extracted in accordance with the Image Biomarker Standardization Initiative (IBSI) standards (37), which include first-order histogram features characterizing voxel intensity distributions (mean, variance, skewness, kurtosis, and homogeneity, among other statistical measures), second-texture features for characterizing differences in internal heterogeneity [gray level co-occurrence matrix (GLCM), gray-level size zone (GLSZM), gray-level run-length matrix (GLRLM), neighboring gray-tone difference matrix (NGTDM), and gray-level dependence matrix (GLDM)], shape characteristics (both 2D and 3D), and higher-order filter transform characterization (wavelet features). To ensure the reproducibility of the results, resampling and z-score normalization were performed on the images and data. To remove dimensionality differences, all data were normalized to the 0-to-1 range via min-max normalization. The binwidth was set to 25. The radiomics features extracted are listed in the supplementary file (https://cdn.amegroups.cn/static/public/tp-24-219-1.docx).

Intraobserver and interobserver agreement

Physician 1, with 11 years of professional experience, performed ROI delineation twice within a week to analyze intragroup consistency, and physician 2, with 5 years of professional experience, independently performed the same delineation once at the same time to analyze intergroup consistency. The Dice coefficient was used to evaluate the overlap between the ROIs, which was calculated using the SimpleITK routine in Python. The extracted features were compared and analyzed to measure the intraobserver and interobserver agreement. The intraclass correlation coefficient (ICC) (38) was used to assess the consistency to ensure the reproducibility of characteristics. An ICC score ≥ 0.75 was considered to have good agreement.

Feature selection and dimensionality reduction

Morphometry features were analyzed via univariate significance analysis to identify the features that were significantly different. To avoid the curse of dimensionality and reduce the bias from abundant radiomics features in model construction, feature selection and dimensionality reduction were performed. First, normality and homogeneity of variance tests were performed, and significant features were selected via the independent samples *t*-test or Mann-Whitney test. Second, the features screened by the test were further reduced and selected to improve the accuracy and robustness based on least absolute shrinkage and selection operator (LASSO) regression (19,39). High-dimensional data with small samples are widely applied in LASSO regression, then LASSO regression was performed with the minimum criterion or one standard error (1-SE) criterion. Ten-fold cross-validation was applied during the regression process, with an adjusted the lambda (λ). Consequently, the coefficients of unimportant features shrank to zero, and finally the significant features with nonzero coefficients were obtained.

Model construction and evaluation

The morphological models, radiomics models, and merged models were constructed, which included multiple logistic regression (MLR) and support vector machine (SVM). MLR and SVM were used to assess the potential imaging markers. The MLR model was built with backward stepwise regression. The SVM model was constructed with radial basis function (RBF). The optimizing the Gaussian kernel size ($\gamma \in [0.001, 1]$) and regularization parameters ($C \in [1, 10{,}000]$) were used to improve the stability of the SVM model through five fold cross-validation to select the best-performing model. Previous studies have shown that SVM algorithms perform well in small-sample data and have excellent performance in medical image analysis (19,40,41). Finally, the models were evaluated, which included calculating the area under the receiver operating characteristic curve (AUC), positive predictive value (PPV),

Table 1 Comparison of demographic and morphologic features between the TOF and control groups

Variable	Total (n=62)	Group		P
		Control (n=29)	TOF (n=33)	
Age (years) (preschool)	4.14±1.18	4.42±0.91	3.89±1.33	0.10
GMV (cm^3)	703.89±62.11	737.72±55.22	674.15±52.31	<0.001
WMV (cm^3)	384.27±50.29	412.28±42.83	359.67±43.37	<0.001
TIV (cm^3)	1,323.77±126.00	1,392.48±123.04	1,263.39±94.75	<0.001
Thickness (mm)	3.02±0.10	2.99±0.08	3.04±0.11	0.046
CSF (mL)	234.97±43.40	241.93±44.75	228.85±41.89	0.24
Gender				0.38
Male	37 (59.68)	19 (65.52)	18 (54.55)	
Female	25 (40.32)	10 (34.48)	15 (45.45)	

Continuous variables are expressed as the mean ± standard deviation according to the distribution of the data, and categorical variables are expressed as numbers (percentages). TOF, tetralogy of Fallot; GMV, gray-matter volume; WMV, white-matter volume; TIV, total intracranial volume; CSF, cerebrospinal fluid.

negative predictive value (NPV), sensitivity, and specificity. The same modeling and evaluation approach was also used in the validation set. All methods were performed in R version 4.1.0 (The R Foundation for Statistical Computing; https://www.r-project.org/).

Correlations of radiomics features with clinical and neurodevelopment metrics

In this study, the Shapiro-Wilk normality test was used to examine the normality distribution of clinical and neurodevelopmental indicators. Pearson correlation or Spearman correlation analyses were then performed based on the distribution to further characterize the quantitative imaging metrics and neurodevelopmental correlations, in addition to their underlying clinical mechanisms. Furthermore, we corrected for age and sex and used MLR to clarify the relationship between radiomics characteristics, neurodevelopmental score, and clinical indicators, with covariates being controlled for.

Statistical analysis

Statistical analyses were employed using R version 4.2.3 (https://www.r-project.org/). The normality of distributions was evaluated with the Shapiro-Wilk test, while the Bartlett test was employed to check variance homogeneity. Continuous variables are presented as means or medians depending on their distribution and were compared using the independent samples *t*-test or Wilcoxon rank sum test. LASSO regression combined with MLR was executed through the "glmnet" package, and the correlation matrix was depicted using "ggplot2". SVM models were developed using the "e1071" and "pROC" packages, and AdaBoost models were constructed using "adabag". Statistical significance was set at P<0.05. Pearson correlation analyses and Spearman correlation analyses were conducted using the "stats" package in R.

Results

Morphometry and radiomic features

The extracted morphometry features included GMV, WMV, TIV, CSF, and cortical thickness (*Table 1*). Results showed that children with TOF exhibited significant differences in GMV, WMV, TIV, and thickness characteristics compared to controls. Meanwhile, 851 radiomics features were extracted from the T1-3D image of each sample based on Pyradiomics, including first-order statistics (18 features), shape-based (14 features), GLCM (24 features), (16 features), GLSZM (16 features), NGTDM (5 features), GLDM (14 features), and wavelet (744 features).

Intra-observer and inter-observer agreement

The median intersection over union (IoU) for intraobserver

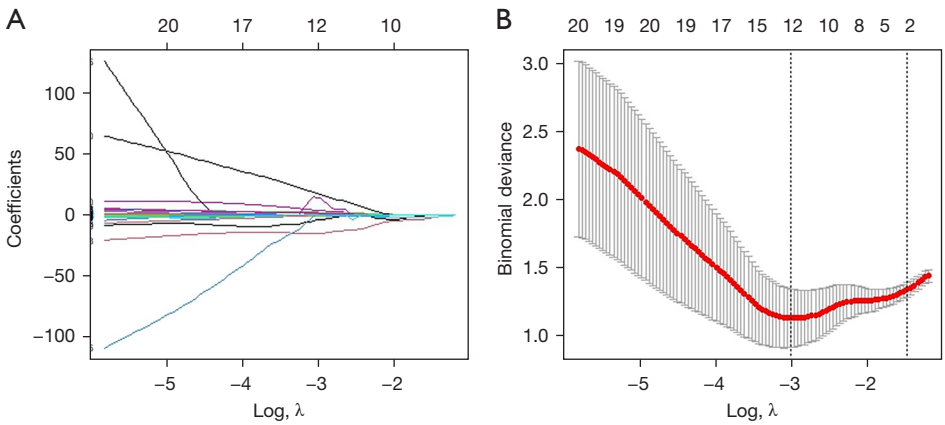

Figure 3 Feature selection by LASSO regression. (A) LASSO coefficient indicated that important features tended to 0 with increasing lambda. (B) The deviance was determined by adjusting the optimal regularization parameters (λ) based on 10-fold cross-validation. The left dashed line delineates the minimum norm, and the right indicates 1-standard error norm (1-SE). This study used the minimum norm. LASSO, least absolute shrinkage and selection operator.

ROI overlap was 95%, with an interquartile range (IQR) of 94% to 96%. For interobserver ROI overlap, the median IoU was 84%, with an IQR of 79% to 85%.

For intraobserver agreement, the agreement rate of all 851 features reached 97.4% (mean ICC =0.961, median ICC =0.988). For interobserver agreement, all 851 features reached 85% agreement (mean ICC =0.899, median ICC =0.966). We found that the 22 features with the poor intraobserver agreement were included in the features with an interobserver agreement.

Feature selection and dimensionality reduction

The morphometry features, including GMV, WMV, TIV, and thickness, which showed significant differences, were selected through univariate analysis.

For high-dimensional radiomics features, a total of 496 features showed a Gaussian distribution with homogeneity, among which 486 were found to be significant according to the independent samples *t*-test. For the remaining features, 77 features showed significant differences according to Mann-Whitney tests. Subsequently, all significant features were subjected to LASSO regression. Eventually, 12 features were retained by LASSO, and 10-fold cross-validation was performed with the best-tuned regularization parameter λ of 0.049 under the minimum criterion. *Figure 3*. illustrates the feature selection process using LASSO. The significant features identified after selection and dimensionality reduction are presented in *Table 2*, in which "Image type" indicates whether the extracted radiomics features were transformed by advanced filtering.

Model construction and evaluation

Both morphological models and radiomics models achieved excellent performance, and notably, the merged models were superior to any single model.

For morphological models in the training cohort, the AUC of the SVM was 80.3% (95% CI: 68.9–91.6%) and that of MLR was 80.8% (95% CI: 70.0–91.6%), while the performances of the validation cohort were 75.6% (95% CI: 53.8–97.8%) and 79.2% (95% CI: 61.0–97.3%), respectively.

For radiomics models, the SVM model showed excellent performance, with an AUC of 91.5% (95% CI: 83.9–99.2%); the optimal γ value of RBF was 0.001 and that of C was 1,000. The MLR model demonstrated strong performance, with an AUC of 88.5% (95% CI: 80.2–96.9%). Similarly, the validation set indicated the model's potential effectiveness, with the SVM model achieving an AUC of 91.7% (95% CI: 76.5–100%) and the MLR model achieving an AUC of 88.1% (95% CI: 73.0–100%).

Meanwhile, the merged models integrating superficial morphological features with deep radiomics features yielded an AUC of 92.2% (95% CI: 84.9–99.4%) for SVM in the training set and an AUC of 91.7% (95% CI: 76.5–100%) in the test set; meanwhile, the MLR had an AUC of 88.8% (95% CI: 80.5–97.1%) in the training cohort and 90.0%

Table 2 Significance features selected after dimensionality reduction

Order	Image type	Feature type	Radiomics feature
1	Original	Shape	Maximum 3D diameter
2	Wavelet-LLH	First order	Maximum
3	Wavelet-LHL	First order	Kurtosis
4	Wavelet-LHH	First order	Mean
5	Wavelet-HLH	GLRLM	Long-run emphasis
6	Wavelet-HHL	First order	Median
7	Wavelet-HHL	GLSZM	Small-area low-gray-level emphasis
8	Wavelet-HHH	First order	Maximum
9	Wavelet-HHH	First order	Mean
10	Wavelet-HHH	GLRLM	Run percentage
11	Wavelet-LLL	First order	Maximum
12	Wavelet-LLL	GLSZM	Size zone nonuniformity

GLSZM, gray-level size zone matrix; GLRLM, gray-level run-length matrix.

Table 3 The performance of machine learning models

	Models	AUC	Accuracy	Sensitivity	Specificity	PPV	NPV
Radiomics							
Training cohort (N=36)	SVM	0.915	0.855	0.879	0.828	0.853	0.857
	MLR	0.885	0.823	0.849	0.793	0.824	0.821
Test cohort (N=26)	SVM	0.917	0.885	0.857	0.917	0.923	0.846
	MLR	0.881	0.808	0.786	0.833	0.846	0.769
Morphometry							
Training cohort (N=36)	SVM	0.803	0.774	0.818	0.724	0.771	0.778
	MLR	0.808	0.726	0.758	0.690	0.735	0.714
Test cohort (N=26)	SVM	0.756	0.769	0.786	0.750	0.786	0.750
	MLR	0.792	0.700	0.714	0.667	0.714	0.667
Merged							
Training cohort (N=36)	SVM	0.922	0.871	0.878	0.862	0.878	0.862
	MLR	0.888	0.800	0.848	0.724	0.777	0.808
Test cohort (N=26)	SVM	0.917	0.885	0.857	0.916	0.923	0.846
	MLR	0.900	0.808	0.786	0.833	0.846	0.769

AUC, area under the receiver operating characteristic curve; PPV, positive predictive value; NPV, negative predictive value; SVM, support vector machine; MLR, multivariable logistic regression.

(95% CI: 75.2–100%) in the test cohort. All the models' specific evaluation results are shown in *Table 3*. The performances of the merged model, the radiomics model, and the structure model with MLR are shown in *Figure 4*.

Correlations of morphological features with clinical and neurodevelopment metrics

The morphological features were correlated with

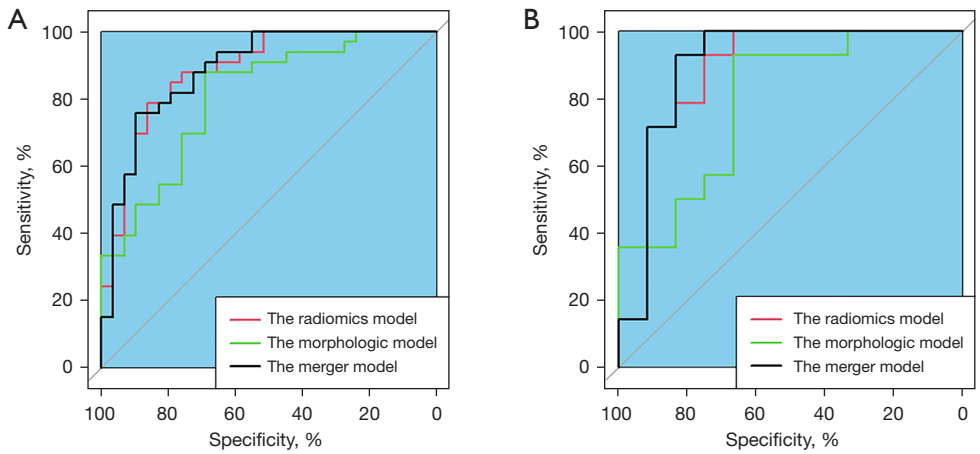

Figure 4 The AUC curve of the merger model, the radiomics model, and the morphologic model. (A) The training set ($AUC_{radiomics}$ =88.5%, $AUC_{morphologic}$ =80.8%, AUC_{merger} =88.8%) and (B) the validation set ($AUC_{radiomics}$ =88.1%, $AUC_{morphologic}$ =79.2%, AUC_{merger} =90.0%).

Table 4 Correlations of morphological features with neurodevelopment metrics

Feature	VCI	VSI	WMI	FSIQ	VAI	NVI	GAI
GMV							
t	0.26	0.36	0.44*	0.36	0.23	0.40*	0.28
P	0.20	0.07	0.03	0.07	0.26	0.04	0.16
WMV							
t	0.30	0.28	0.46*	0.35	0.38	0.32	0.29
P	0.14	0.17	0.02	0.08	0.06	0.11	0.15
TIV							
t	0.17	0.25	0.42*	0.22	0.20	0.33	0.15
P	0.39	0.22	0.03	0.27	0.32	0.10	0.47
Thickness							
t	−0.37	−0.06	−0.41*	−0.29	−0.30	−0.24	−0.23
P	0.06	0.79	0.04	0.16	0.14	0.24	0.26

*, P<0.05. VCI, verbal comprehension index; VSI, visual-spatial index; WMI, working memory index; FSIQ, full scales intelligence quotient; VAI, vocabulary comprehension index; NVI, nonverbal index; GAI, general ability index; GMV, gray-matter volume; WMV, white-matter volume; TIV, total intracranial volume.

neurodevelopmental scales and clinical features, as shown in *Tables 4,5*. Notably, there were differences in structural features and WMI. WMI was significantly associated with GMV (P=0.03; *t*=0.44), WMV (P=0.02; *t*=0.46), TIV (P=0.03; *t*=0.42), and thickness (P=0.04; *t*=–0.41). Meanwhile, VSD was significantly associated with GMV (P=0.01; *t*=0.45), WMV (P<0.001; *t*=0.58), TIV (P=0.04; *t*=0.36), and thickness (P=0.04; *t*=0.35). Significant differences remained after regression correction for age and sex.

Correlations of radiomics features with clinical and neurodevelopment metrics

Radiomics signatures were found to be associated with neurodevelopment and clinical metrics (*Figure 5* and Table S1). Correlation of significance features with neurodevelopmental scales was further assessed to be able to identify quantitative imaging features associated with different cognitive functions that could noninvasively

Table 5 Correlations of morphological features with clinical metrics

Feature	ME	SEL	MAP	ORA	McGoon	SpO_2	VSD	BMI	CPB time	ACC time
GMV										
t	0.01	0.08	0.19	0.02	0.03	0.14	0.45*	0.25	−0.18	−0.04
P	0.96	0.66	0.36	0.89	0.89	0.44	0.01	0.20	0.31	0.84
WMV										
t	0.09	0.11	0.04	0.14	0.05	0.21	0.58**	0.17	−0.32	−0.21
P	0.62	0.57	0.86	0.44	0.80	0.24	<0.001	0.39	0.07	0.25
TIV										
t	0.06	0.12	0.17	0.11	0.07	0.06	0.36*	0.22	−0.21	−0.06
P	0.77	0.53	0.41	0.53	0.72	0.76	0.04	0.27	0.24	0.72
Thickness										
t	0.12	0.33	0.12	0.41*	0.03	0.02	0.35	0.24	0.32	0.24
P	0.53	0.07	0.54	0.02	0.87	0.92	0.04	0.23	0.07	0.18

*, P<0.05; **, P<0.001. ME, maternal education; SEL, socioeconomic level; MAP, maternal age at pregnancy; ORA, overriding aorta; SPO_2, pulse oxygen saturation; VSD, ventricular septal defect; BMI, body mass index; CPB, cardiopulmonary bypass; ACC, aortic cross-clamp; GMV, gray-matter volume; WMV, white-matter volume; TIV, total intracranial volume.

probe for identifying markers of developmental disorders. This could establish the foundation for exploring the neurodevelopmental mechanisms of TOF. Overall, the texture features after wavelet transform indicated high heterogeneity, with wavelet-High-High-Low (HHL)-GLSZM-small-area-low-gray-level-emphasis (SAGLE) showing a significant correlation with the neurodevelopmental scale (*Figure 6A*). Similarly, the first-order features after wavelet transformation [wavelet-Low-High-Low (LHL)-first-order-kurtosis], characterizing heterogeneous differences, also showed significant correlations with neurodevelopmental indicators. The SAGLE feature of GLSZM, characterized by small areas and high heterogeneity, was negatively correlated with SpO_2 (r=−0.433; P=0.02) and positively correlated with VSD (r=0.302; P=0.09), CPB time (r=0.349; P=0.046), and ACC time (r=0.397; P=0.02) (*Figure 6B*). These findings suggest that brain heterogeneity in TOF children may be associated with the severity of the condition and hypoxia during surgery. Additionally, the rough low heterogeneity of long-run emphasis (LRE) from GLRLM was negatively correlated with ORA (r=−0.448; P=0.009) and positively correlated with the McGoon index (r=0.388; P=0.03) (*Figure 6C*). This implies that brain heterogeneity in TOF may be related to the extent of aortic and pulmonary malformations. Similarly, the run percentage from GLRLM, representing high heterogeneity, was positively correlated with ORA (r=0.401; P=0.02) and negatively correlated with the McGoon index (r=−0.402; P=0.03). These results are illustrated in *Figure 6*, with details parameters and explanations provided in Table S1.

Furthermore, MLR analyses of radiomics characteristics with scale scores and clinical indicators were conducted, and the results showed that after correction for age and gender, there was still a significant negative correlation between wavelet-HHL-GLSZM-SAGLE and FSIQ. The results are summarized in Table S2 in the Supplementary Material.

Discussion

TOF is the most common cyanotic CHD in children. Preschool age is a critical period for growth and development, making it highly significant to investigate whether children with CHD exhibit neurodevelopmental abnormalities and to explore the underlying biological mechanisms driving these neurodevelopmental changes. However, most previous studies have concentrated on assessing the TOF neurodevelopment based on brain superficial morphometric features from sMRI (42-44). Our study showed that the sensitivity of deep quantitative features from radiomics (AUC =91.5%) was higher than that of visually assessed morphometric features (AUC

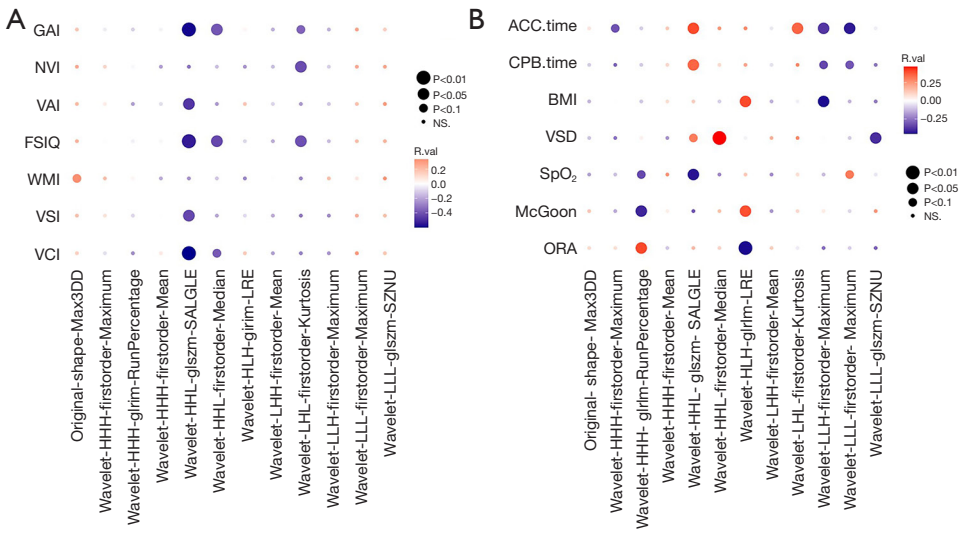

Figure 5 Correlation bubble map of neurodevelopmental scales (A)/clinical metrics (B) and radiomics signatures. The color bar on the right represents the size of the correlation coefficient; the size of the ball represents a significant difference. GAI, general ability index; NVI, non-verbal index; VAI, verbal reception index; FSIQ, full scales intelligence quotient; WMI, working memory index; VSI, visual spatial index; VCI, verbal comprehension index; ACC, aortic cross-clamp; CPB, cardiopulmonary bypass; BMI, body mass index; VSD, ventricular septal defect; SPO_2, pulse oxygen saturation; ORA, overriding aorta; SALGLE, small area low gray level emphasis; LRE, long-run emphasis; SZNU, size zone nonuniformity normalized.

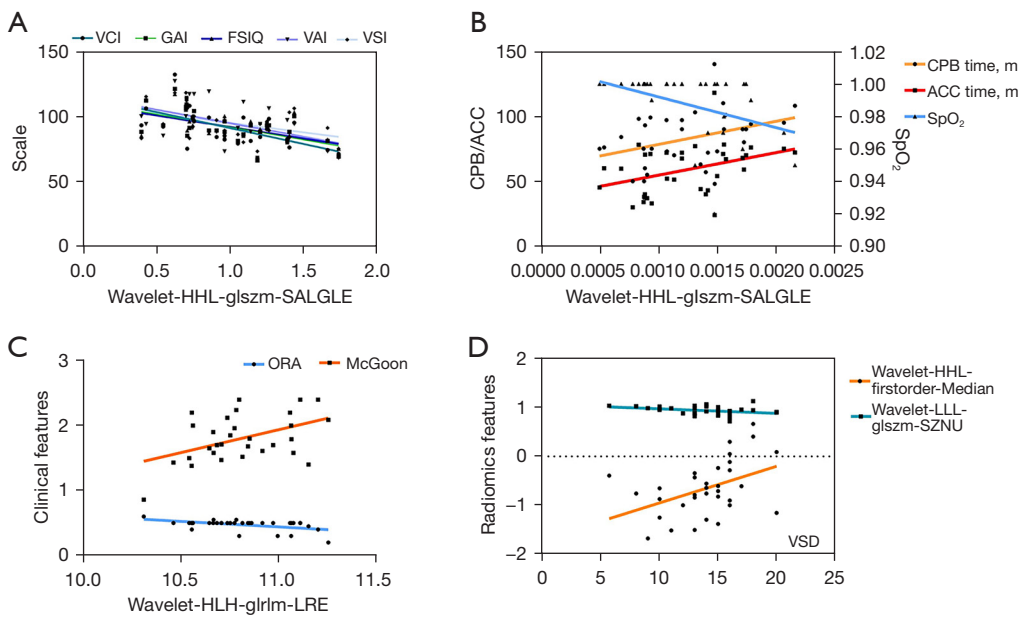

Figure 6 The scatter plots of the radiomics features and neurodevelopmental scales/clinical metrics. VCI, verbal comprehension index; GAI, general ability index; FSIQ, full scales intelligence quotient; VAI, verbal reception index; VSI, visual spatial index; CPB, cardiopulmonary bypass; ACC, aortic cross-clamp; SpO_2, pulse oxygen saturation; ORA, overriding aorta; SALGLE, small area low gray level emphasis; LRE, long-run emphasis; VSD, ventricular septal defect; SZNU, size zone nonuniformity normalized.

=80.3%), which coincides with other research (26). Moreover, radiomics combined with morphometric features could achieve optimal results. Radiomics research has the advantages of being noninvasive and easily accessible, making it particularly suitable for pediatric populations. Therefore, the combination of radiomics and sMRI is expected to become a novel, easy-to-access method for guiding precise diagnosis in clinical practice.

As for morphological characteristics, this study found that the GMV, WMV, TIV, and cortical thickness of the TOF group were significantly different from those of the normal group. Additionally, the brain volume and cortical thickness of children with TOF were smaller than those of healthy controls, which is consistent with previous findings (34). Moreover, there is evidence that changes in thickness can lead to cognitive decline (45).

Radiomics can leverage the potentially significant features of images, which can provide complementary information for distinguishing superficial structures. Wavelet transform decomposes images into various frequency subbands, facilitating the extraction of features that capture both fine and coarse details. The prominent features in this study included first-order features and texture features from wavelet transform, which is consistent with other studies that evaluated neurodevelopment (24,46), indicating that these radiomics features are imaging markers associated with neurodevelopment. Texture features, which reflect the roughness and fineness of MR images, can indicate the heterogeneity of images. The smaller the area is, the finer the image texture, which correlates with higher biological heterogeneity. In the context of lesions, this typically indicates increased malignancy; conversely, larger, less textured areas suggest a more benign nature. While GLSZM represents the size and number of connected domains of all gray levels in the image, GLRLM characterizes the length and number information of the "run" of all gray levels in the image. These features are also significant in the prognosis of neurodevelopment in preterm infants, white-matter abnormalities, and tumors. GLRLM features extracted from multiparametric MRI have been proven valuable for the early identification of disease (11). The GLRLM signature extracted from fluorine-18 fluorodeoxyglucose positron emission tomography (^{18}F-FDG-PET) has also been shown capable of distinguishing primary central nervous system lymphoma from glioblastoma multiforme (GBM) (47). Shu *et al.* found that texture-based radiomics features of whole-brain WM could be used to predict the progression of white-matter hyperintensities (46); Wagner *et al.* predicted adverse neurodevelopmental outcomes of extremely preterm neonates based on MRI radiomics, thus further confirming the importance of GLSZM features in motor outcome prediction (25). Therefore, according to our findings, these factors may also be the potential causes of the neurodevelopmental abnormalities of TOF. Hypoxia or white-matter injury during surgery leads to adverse neurodevelopmental outcomes, which may be one of the explanations for our findings.

Our study demonstrated that novel radiomics frames including radiomics signatures and morphologic MRI signatures are effective in exploring neurodevelopment in patients with TOF. Radiomics and morphometry features provide a comprehensive view of brain development from both macro- and microstructure perspective. These results might also aid in developing a noninvasive method for neurodevelopmental prognosis. Our study provides a novel concept for the prediction of neurodevelopmental prognosis in children, and we showed that a machine learning model combining radiomics features and MRI morphometry features can accurately predict neurodevelopment in patients with TOF.

Interpretability is a substantial obstacle between radiomics and their clinical application (48), and understanding the underlying biological mechanisms of diseases is of great significance to the clinical application of radiomics (49,50). It is worth mentioning that our study explored the interpretability of radiomics features by evaluating the correlation of significant radiomics features with neurodevelopmental scales and clinical metrics, which could better reflect the clinical biological mechanisms of neurodevelopmental changes in TOF. In recent years, radiomics has been widely applied to various diseases. This study further examined the relevance of clinical scale information by identifying imaging markers, which could be helpful in clarifying the related internal biological mechanism, enhancing clinical interpretability, and laying the foundation for further clinical diagnosis. We found that both the clinical intelligence scale and the clinical indicators each corresponded with radiomics features. There was a significant negative correlation between texture features and neurodevelopmental scales, indicating the high heterogeneity of brain structures. Radiomics features indicating high heterogeneity were significantly positively correlated with clinical indicators of hypoxia and deformities, suggesting that the heterogeneity of brain development in TOF may be attributable to the severity of the lesion itself and hypoxia, which is consistent with

previous speculation on biological mechanisms (42).

In the bulk of related research, especially that on brain neurodevelopment, complex sequences, such as Blood Oxygen Level Dependent (BOLD), diffusion tensor imaging (DTI), and arterial spin labeling (ASL), increase the assessment time in children, have poor compliance, and hamper image quality, and some sequences are not routine clinical sequences. In this study, clinical routine sequences were combined with radiomics features to leverage the ease of conventional MRI sequences.

Some limitations of our study should be addressed. First, the small sample size was small (M=62). Because this was a neurodevelopmental study of congenital disorders, neurodevelopmental scales and clinical demographics needed to be collected and the image quality of MR scanning ensured. Therefore, a large-sample analysis in the short term was impracticable. Further validation with a larger data set is needed before clinical application is possible. Moreover, additional external validation with cases from different institutions can improve the generalization of the model. Second, longer follow-up of patients is necessary to track their long-term neurodevelopment, identify additional possible risk factors, and develop effective early interventions. Our group is continuing to follow-up on infants and children who undergo TOF surgery. Finally, in-depth exploration of the specific biological mechanism of the differences in brain development, which requires more adequate clinical, pathological, genetic, and other indicators and long-term follow-up, should be the focus of future research.

Interestingly, we also included parental education, educational attainment, and age at conception among the clinical indicators that are considered likely to be associated with neurodevelopment and found no significant associations before or after correction. Whether this is related to the small sample or based on the nature of the disease mechanisms requires further discussion.

Conclusions

Radiomics combined with sMRI features can be used as noninvasive imaging markers to identify the differences in neurodevelopment in preschool children with TOF. Therefore, the merger of radiomics features with superficial morphological features to derive deep radiomics features can be used to evaluate the neurodevelopment of children with TOF. Moreover, this may be able to generate complementary information on macrostructure and microstructure and thus additional provide references for clinical decision-making.

Acknowledgments

Funding: This study was supported by the Six Talent Peaks Project in Jiangsu Province, CN (No. WSN-192), the China and Jiangsu Commission of Health CN (No. LGY2019009), National Natural Youth Training Program, Children's Hospital of Nanjing Medical University (No. QNPY2024005), and the Science and Technology Development Fund Surface Projects in Nanjing Medical University (No. NMUB20220024).

Footnote

Reporting Checklist: The authors have completed the TRIPOD reporting checklist. Available at https://tp.amegroups.com/article/view/10.21037/tp-24-219/rc

Data Sharing Statement: Available at https://tp.amegroups.com/article/view/10.21037/tp-24-219/dss

Peer Review File: Available at https://tp.amegroups.com/article/view/10.21037/tp-24-219/prf

Conflicts of Interest: All authors have completed the ICMJE uniform disclosure form (available at https://tp.amegroups.com/article/view/10.21037/tp-24-219/coif). The authors have no conflicts of interest to declare.

Ethical Statement: The authors are accountable for all aspects of the work in ensuring that questions related to the accuracy or integrity of any part of the work are appropriately investigated and resolved. The study was conducted in accordance with the Declaration of Helsinki (as revised in 2013). The study was approved by the Ethics Committee of the Children's Hospital of Nanjing Medical University (No. 201907212-1), and informed consent was obtained from all the patients' parents or legal guardians.

References

1. Xi L, Xiang M, Wu C, et al. Adverse events after repair of tetralogy of Fallot: prediction models by machine learning of a retrospective cohort study in western China. Transl Pediatr 2023;12:125-36.
2. Vedovelli L, Cogo P, Cainelli E, et al. Pre-surgery urine metabolomics may predict late neurodevelopmental outcome in children with congenital heart disease. Heliyon 2019;5:e02547.
3. Du J, Liu H, Wang P, et al. Identification and analysis of inflammation-related biomarkers in tetralogy of Fallot. Transl Pediatr 2024;13:1033-50.
4. Sood E, Newburger JW, Anixt JS, et al. Neurodevelopmental Outcomes for Individuals With Congenital Heart Disease: Updates in Neuroprotection, Risk-Stratification, Evaluation, and Management: A Scientific Statement From the American Heart Association. Circulation 2024;149:e997-e1022.
5. White BR, Rogers LS, Kirschen MP. Recent advances in our understanding of neurodevelopmental outcomes in congenital heart disease. Curr Opin Pediatr 2019;31:783-8.
6. Vena F, Manganaro L, D'Ambrosio V, et al. Neuroimaging and Cerebrovascular Changes in Fetuses with Complex Congenital Heart Disease. J Clin Med 2022;11:6740.
7. Song Y, Wen C, Pan Y, et al. Development and validation of a predictive model for low cardiac output syndrome after surgical repair of tetralogy of Fallot. Transl Pediatr 2023;12:1110-20.
8. Peyvandi S, Latal B, Miller SP, et al. The neonatal brain in critical congenital heart disease: Insights and future directions. Neuroimage 2019;185:776-82.
9. Peyvandi S, Rollins C. Fetal Brain Development in Congenital Heart Disease. Can J Cardiol 2023;39:115-22.
10. Bonthrone AF, Stegeman R, Feldmann M, et al. Risk Factors for Perioperative Brain Lesions in Infants With Congenital Heart Disease: A European Collaboration. Stroke 2022;53:3652-61.
11. Chen X, Li W, Wang F, et al. Early recognition of necrotizing pneumonia in children based on non-contrast-enhanced computed tomography radiomics signatures. Transl Pediatr 2021;10:1542-51.
12. Ding H, Chen X, Wang H, et al. Identifying immunodeficiency status in children with pulmonary tuberculosis: using radiomics approach based on un-enhanced chest computed tomography. Transl Pediatr 2023;12:2191-202.
13. Lambin P, Leijenaar RTH, Deist TM, et al. Radiomics: the bridge between medical imaging and personalized medicine. Nat Rev Clin Oncol 2017;14:749-62.
14. Si J, Wang H, Xie M, et al. Distinguishing diffuse large B-cell lymphoma from Hodgkin's lymphoma in children using an enhanced computed tomography radiomics approach. Transl Pediatr 2024;13:716-26.
15. Su GH, Xiao Y, Jiang L, et al. Radiomics features for assessing tumor-infiltrating lymphocytes correlate with molecular traits of triple-negative breast cancer. J Transl Med 2022;20:471.
16. Zhang Y, You C, Pei Y, et al. Integration of radiogenomic features for early prediction of pathological complete response in patients with triple-negative breast cancer and identification of potential therapeutic targets. J Transl Med 2022;20:256.
17. Li L, Hou M, Fang S. Application of colony-stimulating factor 3 in determining the prognosis of high-grade gliomas based on magnetic resonance imaging radiomics. Heliyon 2023;9:e15325.
18. Chen M, Cao J, Hu J, et al. Clinical-Radiomic Analysis for Pretreatment Prediction of Objective Response to First Transarterial Chemoembolization in Hepatocellular Carcinoma. Liver Cancer 2021;10:38-51.
19. Chen Y, Chen TW, Wu CQ, et al. Radiomics model of contrast-enhanced computed tomography for predicting the recurrence of acute pancreatitis. Eur Radiol 2019;29:4408-17.
20. Bera K, Braman N, Gupta A, et al. Predicting cancer outcomes with radiomics and artificial intelligence in radiology. Nat Rev Clin Oncol 2022;19:132-46.
21. Silvestri GA, Jett JR. The Intersection of Lung Cancer Screening, Radiomics, and Artificial Intelligence: Can One Scan Really Predict the Future Development of Lung Cancer? J Clin Oncol 2023;41:2141-3.
22. Shi D, Ren Z, Zhang H, et al. Amplitude of low-frequency fluctuation-based regional radiomics similarity network: Biomarker for Parkinson's disease. Heliyon 2023;9:e14325.
23. Cui H, Sun Y, Zhao D, et al. Radiogenomic analysis of prediction HER2 status in breast cancer by linking ultrasound radiomic feature module with biological functions. J Transl Med 2023;21:44.
24. Shin Y, Nam Y, Shin T, et al. Brain MRI radiomics analysis may predict poor psychomotor outcome in preterm

neonates. Eur Radiol 2021;31:6147-55.
25. Wagner MW, So D, Guo T, et al. MRI based radiomics enhances prediction of neurodevelopmental outcome in very preterm neonates. Sci Rep 2022;12:11872.
26. Shi L, Liu X, Wu K, et al. Surface values, volumetric measurements and radiomics of structural MRI for the diagnosis and subtyping of attention-deficit/hyperactivity disorder. Eur J Neurosci 2021;54:7654-67.
27. Wang M, Liu H, Liu C, et al. Prediction of adverse motor outcome for neonates with punctate white matter lesions by MRI images using radiomics strategy: protocol for a prospective cohort multicentre study. BMJ Open 2019;9:e023157.
28. Bonthrone AF, Kelly CJ, Ng IHX, et al. MRI studies of brain size and growth in individuals with congenital heart disease. Transl Pediatr 2021;10:2171-81.
29. Shin NY, Bang M, Yoo SW, et al. Cortical Thickness from MRI to Predict Conversion from Mild Cognitive Impairment to Dementia in Parkinson Disease: A Machine Learning-based Model. Radiology 2021;300:390-9.
30. Morton SU, Maleyeff L, Wypij D, et al. Abnormal Left-Hemispheric Sulcal Patterns Correlate with Neurodevelopmental Outcomes in Subjects with Single Ventricular Congenital Heart Disease. Cereb Cortex 2020;30:476-87.
31. Aleksonis HA, King TZ. Relationships Among Structural Neuroimaging and Neurocognitive Outcomes in Adolescents and Young Adults with Congenital Heart Disease: A Systematic Review. Neuropsychol Rev 2023;33:432-58.
32. Dhari Z, Leonetti C, Lin S, et al. Impact of Cardiopulmonary Bypass on Neurogenesis and Cortical Maturation. Ann Neurol 2021;90:913-26.
33. Claessens NHP, Breur JMPJ, Groenendaal F, et al. Brain microstructural development in neonates with critical congenital heart disease: An atlas-based diffusion tensor imaging study. Neuroimage Clin 2019;21:101672.
34. Sadhwani A, Wypij D, Rofeberg V, et al. Fetal Brain Volume Predicts Neurodevelopment in Congenital Heart Disease. Circulation 2022;145:1108-19.
35. Syeda MM, Climie EA. Test Review: Wechsler Preschool and Primary Scale of Intelligence–Fourth Edition. J Psychoeduc Assess 2014;32:265-72.
36. Gaser C, Dahnke R, Thompson PM, et al. CAT: A Computational Anatomy Toolbox for the Analysis of Structural MRI Data. bioRxiv 2022. doi: https://doi.org/10.1101/2022.06.11.495736.
37. Zwanenburg A, Vallières M, Abdalah MA, et al. The Image Biomarker Standardization Initiative: Standardized Quantitative Radiomics for High-Throughput Image-based Phenotyping. Radiology 2020;295:328-38.
38. Koo TK, Li MY. A Guideline of Selecting and Reporting Intraclass Correlation Coefficients for Reliability Research. J Chiropr Med 2016;15:155-63.
39. Wang Y, Yang F, Zhu M, et al. Machine Learning Models on ADC Features to Assess Brain Changes of Children With Pierre Robin Sequence. Front Neurol 2021;12:580440.
40. Mukherjee S, Patra A, Khasawneh H, et al. Radiomics-based Machine-learning Models Can Detect Pancreatic Cancer on Prediagnostic Computed Tomography Scans at a Substantial Lead Time Before Clinical Diagnosis. Gastroenterology 2022;163:1435-1446.e3.
41. Neisius U, El-Rewaidy H, Nakamori S, et al. Radiomic Analysis of Myocardial Native T1 Imaging Discriminates Between Hypertensive Heart Disease and Hypertrophic Cardiomyopathy. JACC Cardiovasc Imaging 2019;12:1946-54.
42. Kelly CJ, Christiaens D, Batalle D, et al. Abnormal Microstructural Development of the Cerebral Cortex in Neonates With Congenital Heart Disease Is Associated With Impaired Cerebral Oxygen Delivery. J Am Heart Assoc 2019;8:e009893.
43. Claessens NH, Moeskops P, Buchmann A, et al. Delayed cortical gray matter development in neonates with severe congenital heart disease. Pediatr Res 2016;80:668-74.
44. Ehrler M, von Rhein M, Schlosser L, et al. Microstructural alterations of the corticospinal tract are associated with poor motor function in patients with severe congenital heart disease. Neuroimage Clin 2021;32:102885.
45. Grasby KL, Jahanshad N, Painter JN, et al. The genetic architecture of the human cerebral cortex. Science 2020;367:eaay6690.
46. Shu Z, Xu Y, Shao Y, et al. Radiomics from magnetic resonance imaging may be used to predict the progression of white matter hyperintensities and identify associated risk factors. Eur Radiol 2020;30:3046-58.
47. Kong Z, Jiang C, Zhu R, et al. (18)F-FDG-PET-based radiomics features to distinguish primary central nervous system lymphoma from glioblastoma. Neuroimage Clin 2019;23:101912.
48. Fornacon-Wood I, Mistry H, Ackermann CJ, et al. Reliability and prognostic value of radiomic features are highly dependent on choice of feature extraction platform.

Eur Radiol 2020;30:6241-50.
49. Tomaszewski MR, Gillies RJ. The Biological Meaning of Radiomic Features. Radiology 2021;298:505-16.
50. Huang EP, O'Connor JPB, McShane LM, et al. Criteria for the translation of radiomics into clinically useful tests. Nat Rev Clin Oncol 2023;20:69-82.

(English Language Editor: J. Gray)

Cite this article as: Yang F, Zhong J, Liu P, Yu W, Liu Y, Zhu M, Yang M, Mo X. Radiomics with structural magnetic resonance imaging, surface morphometry features, neurology scales, and clinical metrics to evaluate the neurodevelopment of preschool children with corrected tetralogy of Fallot. Transl Pediatr 2024;13(9):1571-1587. doi: 10.21037/tp-24-219

Supplementary

Table S1 The correlation and explanations between neurodevelopment/clinical metrics and radiomics

Neurodevelopment / clinical Metrics	Radiomics features	*t*	P	Relationship explanations	Biological Conclusion
VCI	Wavelet-HHL-glszm-SALGLE	–0.594**	0.001	The texture features of small areas indicate fine texture and higher heterogeneity, is negative correlation with VCI.	The response appeared to show high heterogeneity affects verbal comprehension and expression.
VSI	Wavelet-HHL-glszm-SALGLE	–0.424*	0.031	Similarly, higher heterogeneity is negative correlation with VCI.	High heterogeneity may affect ability to analyze and organize patterns.
FSIQ	wavelet-HHL-glszm-SALGLE	–0.536**	0.005	Similarly, higher heterogeneity is negative correlation with FSIQ.	High heterogeneity may affect the entire ability, language acquisition, reasoning and expression, analysis and organization, thinking and memory
VAI	wavelet-HHL-glszm-SALGLE	–0.471*	0.015	Similarly, higher heterogeneity is negative correlation with VAI.	High heterogeneity may affect the language accepter ability.
NVI	wavelet-LHL-firstorder-Kurtosis	–0.412*	0.037	Similarly, higher heterogeneity is negative correlation with NVI.	High heterogeneity may affect the ability to react and think about pictorial materials.
GAI	wavelet-HHL-glszm-SALGLE	–0.581**	0.002	Similarly, higher heterogeneity is negative correlation with NVI.	High heterogeneity may affect the general cognitive ability.
ORA	wavelet-HLH-glrlm-LRE	–0.448**	0.009	Lower heterogeneity is negative correlation with Overriding aorta.	High heterogeneity may be affected by hypoxic.
McGoon	wavelet-HLH-glrlm-LRE	0.388*	0.034	Lower heterogeneity is positive correlation with McGoon index.	High heterogeneity may be affected by cardiac anomalies and hypoxic.
SpO2	wavelet-HHL-glszm-SALGLE	–0.433*	0.012	Higher heterogeneity is negative correlation with McGoon index.	High heterogeneity may be affected by hypoxic.
VSD	wavelet-HHL-glszm-SALGLE	0.302	0.088	Higher heterogeneity is positive correlation with ventricular septal defect.	High heterogeneity may be affected by cardiac anomalies.
CPB time	wavelet-HHL-glszm-SALGLE	0.349*	0.046	Higher heterogeneity is positive correlation with Cardiopulmonary Bypass time.	High heterogeneity may be affected by hypoxic.
ACC time	wavelet-HHL-glszm-SALGLE	0.397*	0.022	Higher heterogeneity is positive correlation with aortic cross-clamp time.	High heterogeneity may be affected by hypoxic.
ORA	wavelet-HHH-glrlm-RunPercentage	0.401*	0.021	Higher heterogeneity is positive correlation with Overriding aorta.	High heterogeneity may be affected by cardiac anomalies and hypoxic.
McGoon	wavelet-HHH-glrlm-RunPercentage	–0.402*	0.028	Higher heterogeneity is negative correlation with McGoon index.	High heterogeneity may be affected by hypoxic.

*, P<0.05; **, P<0.001.

https://dx.doi.org/10.21037/tp-24-219

Table S2 Correlations of radiomics features with neurodevelopment metrics (FSIQ)

Variables	β	S.E	*t*	P	β (95% CI)
Intercept	186.46	990.85	0.19	0.854	186.46 (–1755.58 to 2128.50)
Original- shape- Max3DD	0.13	0.51	0.26	0.797	0.13 (–0.86 to 1.13)
Wavelet-LLH-firstorder-Maximum	–0.00	0.00	–0.12	0.905	–0.00 (–0.01 to 0.01)
Wavelet-LHL-firstorder-Kurtosis	0.46	3.95	0.12	0.909	0.46 (–7.27 to 8.19)
Wavelet-LHH-firstorder-Mean	–363.68	390.05	–0.93	0.368	–363.68 (–1128.18 to 400.81)
Wavelet-HLH-glrlm-LRE	–14.29	18.28	–0.78	0.448	–14.29 (–50.11 to 21.54)
Wavelet-HHL-firstorder-Median	–104.22	72.80	–1.43	0.176	–104.22 (–246.91 to 38.47)
Wavelet-HHL- glszm- SALGLE	–15165.89	6942.92	–2.18	0.048	–15165.89 (–28773.76 to –1558.02)
Wavelet-HHH- firstorder- Maximum	–0.04	0.05	–0.74	0.472	–0.04 (–0.14 to 0.06)
Wavelet-HHH-firstorder-Mean	–3286.39	2191.04	–1.50	0.158	–3286.39 (–7580.74 to 1007.97)
Wavelet-HHH- glrlm- RunPercentage	–13.93	1576.90	–0.01	0.993	–13.93 (–3104.59 to 3076.73)
Wavelet-LLL- firstorder- Maximum	0.00	0.01	0.27	0.788	0.00 (–0.02 to 0.03)
Wavelet-LLL- glszm- SZNU	0.00	0.00	1.55	0.144	0.00 (–0.00 to 0.00)

Adjust: gender, age.

https://dx.doi.org/10.21037/tp-24-219